IOP Publishing Biomed. Mater. 15 (2020) 055037 https://doi.org/10.1088/1748-605X/ab99d4

Biomedical Materials

PAPER

Silk fibroin reactive inks for 3D printing crypt-like structures

Danielle L Heichel[1,4], Julia A Tumbic[1,4], Marisa E Boch[2], Anson W K Ma[1,2] and Kelly A Burke[1,2,3]

[1] Polymer Program, Institute of Materials Science, University of Connecticut, Storrs, CT, United States of America
[2] Chemical and Biomolecular Engineering, University of Connecticut, Storrs, CT, United States of America
[3] Biomedical Engineering, University of Connecticut, Storrs, CT, United States of America
[4] These authors have contributed equally to this work.

E-mail: kelly.burke@uconn.edu

RECEIVED
6 April 2020

REVISED
13 May 2020

ACCEPTED FOR PUBLICATION
5 June 2020

PUBLISHED
28 August 2020

Keywords: silk, rheology, 3D printing

Supplementary material for this article is available online

Abstract

A reactive silk fibroin ink formulation designed for extrusion three-dimensional (3D) printing of protein-based hydrogels at room temperature is reported. This work is motivated by the need to produce protein hydrogels that can be printed into complex shapes with long-term stability using extrusion 3D printing at ambient temperature without the need for the addition of nanocomposites, synthetic polymers, or sacrifical templates. Silk fibroin from the *Bombyx mori* silkworm was purified and synthesized into reactive inks by enzyme-catalyzed dityrosine bond formation. Rheological and printing studies showed that tailoring the peroxide concentration in the reactive ink enables the silk to be extruded as a filament and printed into hydrogel constructs, supporting successive printed layers without flow of the construct or loss of desired geometry. To enable success of longer-term *in vitro* studies, 3D printed silk hydrogels were found to display excellent shape retention over time, as evidenced by no change in construct dimensions or topography when maintained for nine weeks in culture medium. Caco-2 (an intestinal epithelial cell line) attachment, proliferation, and tight junction formation on the printed constructs was not found to be affected by the geometry of the constructs tested. Intestinal myofibroblasts encapsulated within reactive silk inks were found to survive shearing during printing and proliferate within the hydrogel constructs. The work here thus provides a suitable route for extrusion 3D printing of protein hydrogel constructs that maintain their shape during printing and culture, and is expected to enable longer-term cellular studies of hydrogel constructs that require complex geometries and/or varying spatial distributions of cells on demand via digital printing.

1. Introduction

Three-dimensional (3D) printing is an additive manufacturing process that is now widely accepted for the bottom-up fabrication of components from different materials, including metals [1, 2], ceramics [3, 4], and polymers [5–7]. Hydrogels are a subclass of polymeric materials that contain polymer chains linked by chemical and/or physical associations into a highly swollen network structure. Hydrogels have long been desired for biomedical applications for their low moduli that can better match the stiffness of soft tissues and their high degrees of hydration that facilitate mass transport through the construct. Additionally, if the crosslinking process is biocompatible, cells can be encapsulated within gel constructs to generate 3D *in vitro* models of tissue, which have potential to better match the *in vivo* function of tissues compared to two-dimensional (2D) culture models [8, 9]. Advancing the physiological relevance of engineered models of human tissue necessitates increased complexity, in terms of both the number of cell types included and the organization of cells within the construct. 3D printing has the capacity to enhance both of these features by dictating complex geometries and by permitting spatial localization of cell types within tissue constructs.

Hydrogels have been 3D printed using different types of methods, including extrusion-based printing [10–12] and FRESH [13] printing. For extrusion-based methods, the printed materials must have low enough viscosity to be pushed through

the printing needle yet need to rapidly reach a large enough viscosity so that they resist flow from the desired printed geometry after deposition. To achieve this, thermoresponsive polymers are frequently employed, such as when constructs are printed into a supporting bath [13]. Reactive polymer solutions have also been investigated for extrusion-based printing. A key challenge with reactive solutions is that viscosity varies during the time course of printing, leading to undesired effects such as heterogeneous material deposition, the need for increasingly large values of extrusion pressure, and the clogging of the printing system. One option to overcome these challenges is to print a shear thinning solution that decreases in viscosity as shear stress increases. This non-Newtonian flow behavior enables extrusion of a liquid-like material that becomes more solid-like once the stress is removed. One important example is the blending of polymers with Laponite clays, which have been shown to serve as effective viscosity modifiers to enable 3D printing of hydrogels [14–16], including silk fibroin [17].

An alternative approach to circumvent the need for thermal adjustments or composite inks is to break the crosslinking up into stages. In the first stage, the reaction is designed to reach an appropriate viscosity to enable extrusion through the print needle and prompt setting of the printed solution. The reaction is also ideally designed to make viscosity invariant with time to eliminate heterogeneity in the printed constructs and the clogging of needles. The second stage consists of a post-print type of crosslinking that locks in the final structure. This process is similar to the extrusion-based printing of polymers that rapidly crosslink once deposited into a printing bath, such as employed for alginate constructs, but is actually different because it employs a chemical reaction to generate a printable gel and the second mode of crosslinking may be more delayed. Two-stage, reactive protein formulations have been reported previously, including gelatin [18–20] modified with methacrylate groups for photocrosslinking after printing, collagen [21] crosslinked by genipin after printing, and fibrin gels [22–24] prepared either by printing fibrinogen and crosslinking with thrombin after printing or by printing thrombin onto deposited fibrinogen layers.

This work sought to develop a reactive ink formulation for silk fibroin (herefter: silk) hydrogels. Silk hydrogels were desired because of their stability for long-term *in vitro* tissue culture, which arises from their lack of recognition sites for human enzymes and their formation of beta sheet secondary structures that act to physically crosslink the material. There are established methods to isolate pure silk fibroin from the cocoons of *Bombyx mori*, the domesticated silkworm [25], and variation of the boil treatment time leads to varying molecular weight of the starting material. Previous work has shown that horseradish peroxidase (HRP) treatment of silk fibroin in the presence of dilute hydrogen peroxide leads to the formation of a hydrogel whose mechanical properties and degradation rate can be tuned by varying the boil treatment time, protein's concentration, and amount of beta sheet within the gel [26].

Silk fibroin hydrogels have subsequently been processed by 3D printing by chemically modifying silk fibroin with methacrylate groups and crosslinking with photocuring [27], by using a sacrifical alginate template [28], or by blending with gelatin [29, 30], hydroxypropyl methyl cellulose (HPMC) [31], or poly(ethylene glycol)[32] or other polyols [33]. In contrast to these previous reports, this work investigated a two-stage crosslinking by partially crosslinking the silk fibroin using HRP, that was found to quickly reach a steady state value for viscosity and display frequency-dependent flow behavior that suggests printability. Though there is another recent report [34] of partially-crosslinked silk fibroin for 3D printing, that work used freeze-drying to lock in the printed structures and is therefore not compatible for gel printing and cell encapsulation, both of which are demonstrated in this work. The rheological characteristics of the inks were characertized and compared to the HRP gels with the one step crosslinking. The reactive inks were found to be superior in terms of printability, and the post processing method was found to stabilize the printed hydrogel constructs without damage to cellular compatibility. This work demonstrates the utility of these constructs in a crypt-like morphology using human intestinal epithelial cells (Caco-2 cell line) and also demonstrates the potential for intestinal myofibroblasts (InMyoFibs) to be encapsulated in the reactive ink hydrogels for a co-culture model.

2. Experimental

2.1. Methods

2.1.1. Reagents

Bombyx mori silkworm cocoons were purchased from Tajima Shoji Co., Ltd. (Tokyo, Japan). Lithium bromide (LiBr, ≥99%), sodium carbonate (Na_2CO_3, ≥99%), HRP (Type VI-A), hydrogen peroxide (H_2O_2, ACS reagent), alginic acid sodium salt (alginate, medium viscosity), calcium chloride ($CaCl_2$, 96.0%) were obtained from Sigma Aldrich (St. Louis, MO). Minimum essential medium (MEM), fetal bovine serum (FBS, qualified), sodium pyruvate, antibiotic-antimycotic (Anti-Anti), non-essential amino acids (NEAA), 4′,6-diamidino-2-phenylindole (DAPI), lactate dehydrogenase (LDH) cytotoxicity assay kit, alamarBlue, regenerated cellulose dialysis tubing (3500 MWCO), 10X phosphate-buffered saline (10X PBS), Dulbecco's PBS (DPBS), 0.25% trypsin-EDTA solution, Calcein AM, Hoechst 33 342, and Triton X-100 were purchased from ThermoFisher (Waltham, MA). Mouse monoclonal antibody to claudin-1 (A-9)

(sc-166 338, FITC conjugated) was purchased from Santa Cruz Biotechnology (Dallas, TX) and used at a 1:50 dilution in 1X PBS. Caco-2 cells were obtained from ATCC (Manassas, VA). Human InMyoFibs and smooth muscle cell growth medium-2 (SmGM-2) were purchased from Lonza (Walkersville, MD). Sylgard 184 was purchased from Ellsworth Adhesives (Germantown, WI). Stainless steel blunt needles (27 G) were obtained from McMaster Carr (Elmhurst, IL). An in-house purification unit was used to obtain ultrapure water (dH_2O, 18 MOhm cm) used in all experiments.

2.1.2. Instruments

Silk and alginate constructs were printed by using a Hyrel 30 M 3D printer (Hyrel 3D, Nocross, GA), and the printer was controlled by Repetrel software (v. 2.855, Hyrel 3D). Time and frequency sweeps were measured using an AR-G2 rheometer (TA Instruments, New Castle, DE), and Trios software (v. 4.3.1, TA Instruments) was used to collect the data. To monitor the secondary structure changes of silk, a Magna 560 Fourier transform infrared (FTIR) spectrometer (Nicolet, Madison, WI), coupled with a diamond attenuated total reflectance (ATR) accessory (Specac, Fort Washington, PA), was used to characterize the amide I region. The beta sheet content was quantified by deconvoluting the amide I region using Origin software (v. 8.1, Northampton, MA). An AmScope ME 520TA Metallurgical microscope (AmScope, Irivine, CA) and AmScope imaging software (v. 3.7, Irvine, CA) was used to quantify construct dimensions (*x*-axis and *y*-axis directions). The depth of the constructs (*z*-axis direction) and the cellular morphology on the constructs were characterized by using Leica SP8 confocal microscope (Leica, Buffalo Drive, IL), and Leica Application Suite X (Leica, v. 3.3.0) was used for acquiring images. The optical and confocal microscopy images were evaluated using Image J (NIH, Bethesda, MD). Cell proliferation and viability were assessed using alamarBlue and LDH assays, and fluorescence and absorbance values were measured using a Synergy HT plate reader (BioTek, Winooski, VT) and Gen5 software (BioTek).

2.2. Silk fibroin extraction and solution preparation

Silk fibroin (SF) was extracted from *B. mori* silk cocoons based on a previously established method [25]. Briefly, silk cocoons were boiled in 0.2 M sodium carbonate solution for 30 min, followed by washing with ultrapure (DI) water. The resulting SF fibers were allowed to dry overnight at room temperature. To prepare the SF solution, the SF fibers were dissolved in 9.3 M LiBr for 4 h at 60 °C. The dissolved fibers were then placed into regenerated cellulose dialysis tubing (MWCO 3500) and dialyzed against DI water at room temperature for 48 h with 6 exchanges. The resulting solution was centrifuged twice at 12 700 *g* for 20 min and was stored at 4 °C.

2.3. SF hydrogel and reactive ink preparation

SF hydrogels (**SF-Gel**) were prepared based on a previous method [26] utilizing HRP and hydrogen peroxide to form dityrosine bonds between tyrosine residues. Briefly, SF solutions containing 1–4 w v^{-1}% SF were prepared by diluting the purified silk fibroin solution. Next, 10 µl of 1000 U ml^{-1} HRP and 10 µl of 165 mM hydrogen peroxide (H_2O_2) were added per 1 ml of SF solution. The reaction was carried out at room temperature or 37 °C. In this work, these fully crosslinked silk hydrogels will be named **SF-Gel-X**, where **X** is the percentage of silk protein in the gel, as expressed in weight/volume.

Reactive silk inks (**SF-Ink**) were prepared by adjusting the volume of hydrogen peroxide that was added to the reacting SF solution. This volume was dependent on SF concentration, where a higher concentration of SF required a higher volume of hydrogen peroxide to form an adequate crosslinking density. For the lowest SF concentration tested, the final H_2O_2 concentration ranged from 0.139 mM to 0.163 mM, and for the highest SF concentration tested, the final H_2O_2 concentration ranged from 0.294 mM to 0.326 mM for 1 ml of SF solution. A table outlining concentrations and volumes of HRP and H_2O_2 added to **SF-Ink** and **SF-Gel** for varying protein concentrations is provided in supporting information (table S1 avaliable online at stacks.iop.org/BMM/15/055037/mmedia). In this work, these partially crosslinked reactive ink formulations will be named **SF-Ink-X**, where **X** is the percentage of silk protein, as expressed in weight/volume.

Alginate inks (**Alg-Ink-3**) were also prepared by partially crosslinking a 3% sodium alginate solution in DI water with 60 mM $CaCl_2$. The final concentration of alginate was 2.65% once mixed with the $CaCl_2$ solution.

2.4. Robotic dispensing and post-printing processing of SF and alginate scaffolds

3D printed gel scaffolds made of 4% or 2% SF (**SF-Gel** or **SF-Ink** series) or 3% alginate were printed at room temperature using a Hyrel System 30 M printer and an EMO-25 printhead. The inks were extruded through a 27 G blunt needle, which corresponds to an inner diameter of approximately 200 µm. Printed materials were dispensed at a speed of 10 mm s^{-1} onto a silicone substrate with a gap size of 200 µm. Construct designs were made using AutoCAD 2016. A G-code of the design was then generated using Slic3 r (v1.2.9). The resulting G-code was used for printing and read with Repetrel (v2.865).

After printing, flat and crypt-like **SF-Ink** scaffolds were further crosslinked at room temperature on the

silicone substrate by applying 50 µl of a dilute hydrogen peroxide solution, the concentration of which was dependent on the original volume of hydrogen peroxide used to prepare the ink (table S1). After crosslinking, the constructs were stored in DI water until needed. The **Alg-Ink** constructs were further crosslinked with 0.1 M $CaCl_2$ at room temperature and were stored in a 0.1 M $CaCl_2$ solution until needed.

2.5. Cell culture

2.5.1. Scaffold preparation

Scaffolds were sterilized for cell culture by soaking the SF constructs in 70% ethanol, and alginate constructs were sterilized in 70% ethanol supplemented with 0.1 M $CaCl_2$ to maintain their shape. The ethanol solutions were exchanged after 1 h, and then the scaffolds in ethanol were placed in the incubator overnight. After sterilizing, the SF scaffolds were washed with DI water, then equilibrated in cell culture medium. The alginate scaffolds were treated similarly, but with 0.1 M $CaCl_2$ supplementation in all solutions. After equilibration, scaffolds were treated with a sterile 200 µg ml^{-1} gelatin and 4 µg ml^{-1} fibronectin solution to facilitate cell attachment. 48-well plates were lined with a silicone layer (Syglard 184) to the bottom of wells to reduce cell adhesion to the plate. The silicone was prepared according to manufacturer's instructions, and the cured elastomer was sterilized using UV light and 70% ethanol. Sterilized and gelatin/fibronectin coated scaffolds were then placed into the wells, and autoclaved silicone rings were placed on top to prevent scaffold movement.

2.5.2. Cell expansion

Caco-2 cells were expanded at 37 °C with 5% CO_2 in tissue culture flasks at an initial seeding density of 4500 cells/cm^2 and passaged at 70%–80% of confluence [35]. The medium consisted of MEM supplemented with 10% FBS, 1% Anti-Anti, 1% NEAA, and 1% sodium pyruvate. Caco-2 cells were harvested at Passage 26 for cell attachment and proliferation experiments. Human InMyoFibs were expanded at an initial density of approximately 2500 cells/cm^2 at 37 °C with 5% CO_2 in SmGM-2. InMyoFibs were used at Passage 6.

2.5.3. Caco-2 seeding onto constructs

The amount of cells to be seeded was determined by calculating the surface area of the SF and alginate printed constructs using data obtained from optical and confocal microscope images. For SF scaffolds with crypt-like morphology, 19 500 cells were seeded, giving a seeding density of approximately 58 000–66 000 cells cm^{-2} for **SF-Ink-4** and 55 000–68 000 cells cm^{-2} for **SF-Ink-2**. To achieve a cell seeding density of approximately 60 000 cells cm^{-2} for **Alg-Ink-3**, 21 400 cells/construct were seeded. Finally, cells were seeded onto tissue culture plastic (TCP) and flat 4% SF and 2% SF constructs at a density of 60 000 cells cm^{-2}. Cells were allowed to attach to the SF and alginate scaffolds for 5 h before flooding the well with medium.

2.5.4. InMyoFib seeding within constructs

4% and 2% SF solutions with 1X PBS, 165 mM H_2O_2, and 1000 U ml^{-1} HRP were sterile-filtered separately through a 0.22 µm polyvinylidene difluoride (PVDF) filter. To encapsulate cells at the desired cell density of 100 000 cells ml^{-1} or 380 000 cells ml^{-1}, cells were resuspended to 5.26×10^6 cells ml^{-1} and 20×10^6 cells ml^{-1}, respectively. To encapsulate myofibroblasts using the two-step crosslinking method, 981 µl of 4% or 2% SF solution containing 1% gelatin and 0.02% fibronectin (percentages are relative to silk content), 2.1 or 2.5 µl H_2O_2 (for 2% and 4% gels, respectively), and 10 µl HRP were mixed together before adding 19 µl of cell suspension to the reacting solution. As above, the cell suspension contains 5.26×10^6 cells ml^{-1} for the gels containing 100 000 cells ml^{-1}, and the cell suspension contains 20×10^6 cells ml^{-1} for the gels containing 380 000 cells ml^{-1}. The reacting solution containing cells was then aliquoted into wells of 48-well plates. The reactive inks were cured at 37 °C for 5–7 min. A sterile dilute solution of H_2O_2 in 1X PBS, the concentration of which was dependent on the initial volume of H_2O_2 used (100 µl of 1.24 mM H_2O_2 for the **SF-Ink-4**; 100 µl of 1.30 mM H_2O_2 for the **SF-Ink-2**), was then added to the partial-gels to finish crosslinking. After curing for 20 min at 37 °C, the dilute H_2O_2 solution was aspirated and replaced with medium. The medium was exchanged after approximately 45 min to ensure removal of residual H_2O_2.

2.6. Material characterization methods

2.6.1. Rheology of SF hydrogels and inks

2.6.1.1. Time sweeps

Gelation kinetics of reacting SF solutions containing water to form fully- and partially-crosslinked 1%–4% SF hydrogels was examined using oscillatory time sweeps on an AR-G2 rheometer. The reacting SF solutions were prepared on ice and loaded onto a Peltier plate set to 5 °C. A 20 mm aluminium plate was used with a gap of 500 µm. For gels prepared using ultrapure water, testing was carried out at 25 °C with a strain of 10% and frequency of 0.2 rad s^{-1}. For gels prepared using 1X PBS, linear viscoelastic measurements were carried out at 37 °C with a strain of 10% and frequency of 0.2 rad s^{-1}. To prevent dehydration of the samples, a solvent trap filled with water was used.

2.6.1.2. Frequency sweeps

Oscillatory frequency sweeps were carried out after the time sweeps (described in Section 2.6.1.1) once the storage modulus of the hydrogel samples had reached a plateau. The purpose of the frequency

sweeps was to characterize gel viscoelasticity as a function of SF concentration and crosslink density. The frequency sweeps on hydrogels containing water were conducted at 25 °C with an applied strain of 10%, while the hydrogels containing 1X PBS were tested at 37 °C with the same strain. The tested frequency range was 0.2–10 rad s^{-1}.

2.6.2. Ditryosine bond formation using fluorescence spectroscopy

To compare the degree of dityrosine formation in the partially crosslinked solutions and the fully crosslinked gels, fluorescence was used. When a sample containing dityrosine bonds is excited at 315 nm, there is a related emission at 400 nm that is directly correlated to the number of dityrosine bonds[36, 37]. Silk solutions at concentrations of 2 w v^{-1}% and 4 w v^{-1}% were diluted from a 5.9 w v^{-1}% silk stock solution, and 100 µl of the solutions were transferred into a black 96-well plate. Partially crosslinked silk samples were prepared by adding 10 µl HRP and 2.15 µl H_2O_2 to the 4 w v^{-1}% SF solutions, and 10 µL and 1.4 µL H_2O_2 to the 2 w v^{-1}% SF solutions. 100 µl of the partially crosslinked SF solutions (**SF-Inks**) were added to the well plate. The fully crosslinked samples (**SF-Gels**) were prepared by adding 10 µl of HRP and 10 µl H_2O_2 to both concentrations of SF, and 100 µl of the solution was transferred to the well plate. Four replicates were run, and solutions were allowed to react at 25 °C for 30 min before measuring fluorescence with a plate reader.

2.6.3. ATR-FTIR

FTIR was used to characterize secondary structure of 1%–4% SF inks and solutions to determine if shearing that occurs during the printing process induces changes in the silk structure. **SF-Inks** were prepared according to the printing procedure above. The corresponding solutions were prepared by simply diluting a stock SF solution with DI water. Samples that were not sheared were gently mixed with a micropipettor before dispensing. Sheared samples were gently mixed prior to manual extrusion through a 27 G blunt needle. All samples were dried at room temperature. FTIR spectra were then acquired on the dried films using an ATR-FTIR equipped with a diamond crystal with 32 scans at a resolution of 4 cm^{-1}. The resulting peaks in the amide I region, which corresponds to approximately 1595–1705 cm^{-1}, were deconvoluted using a previously established method [38].

2.6.4. Optical and fluorescence microscopy

2.6.4.1. Optical microscopy

An AmScope ME 520TA Metallurgical microscope was used to quantify construct dimensions (*x*-axis and *y*-axis directions). Flat and crypt-like acellular constructs were printed and sterilized as described above and then stored in complete cell culture medium over a period of 62 d. The shape retention over time of flat and crypt-like silk hydrogels were assessed by imaging the gels at time points over 62 d and subsequently measuring the side lengths and hole diameters, respectively, with Image J software. For flat hydrogels, horizontal and vertical side lengths were averaged for each sample, and the percent change in side length compared to day 0 were calculated at each time point. For crypt-like hydrogels, the hydrogel was imaged in four quadrants (top left, top right, bottom left, and bottom right), and the hole diameters of all crypts in a scaffold were averaged at each time point.

Optical microscopy was also used to assess changes in printed crypt-like SF constructs that would potentially occur with the post-printing crosslinking and sterilization steps described above, and to examine how these changes would be affected by SF concentration and programmed hole size. Samples made with **SF-Ink-4**, **-3**, and **-2** were printed according to the procedure described above with a programmed hole size of 1000 µm, and subsequently crosslinked and sterilized using the procedures described above. **SF-Ink-3** constructs were also printed with programmed hole sizes of 1200 µm and 700 µm. Red food dye (FD&C Red 40 and 3) was added to the inks to help with visualization. Images were taken of the samples as-printed, crosslinked, and sterilized using the 10X objective, and ImageJ was used to measure diameters of the holes for each sample.

2.6.4.2. Confocal microscopy

Acellular and cell-laden SF scaffolds were imaged using a Leica SP8 confocal microscope. Acellular printed scaffolds were dyed with DAPI in water, and the 405 UV diode was used for imaging. Cell-laden scaffolds were imaged with 0.1 mg ml^{-1} Hoechst and 4 µM Calcein AM in 1X DPBS. The 405 UV diode and 488 nm argon laser were used. Z-stacks were obtained to calculate average depth of crypts in acellular scaffolds and to assess cell morphology and proliferation in the crypts of cell-laden scaffolds. Images of Caco-2-laden scaffolds and Caco-2 cells grown on TCP were acquired on days 1, 8, 15, 22, and 29.

2.6.5. Caco-2 attachment and proliferation on scaffolds

2.6.5.1. Caco-2 attachment

Attachment of Caco-2 cells onto SF hydrogels and TCP was calculated using cell metabolic activity, as measured by an alamarBlue assay run 1 d post-seeding. The alamarBlue working solution was prepared by diluting the reagent 1:10 in Caco-2 medium. The assay was run according to manufacturer's instructions, and fluorescence (Ex 560 nm, Em 590 nm) was normalized to acellular wells for TCP samples and to acellular constructs for SF and alginate. Varying numbers of Caco-2 cells were seeded into TCP wells to generate a standard curve and permit calculation of the number of cells attached to

the constructs. The percentage of cell attachment was calculated by dividing the number of cells measured using the alamarBlue assay by the number of cells seeded.

2.6.5.2. Caco-2 and InMyoFib proliferation

Metabolic activity of Caco-2 cells seeded on constructs was measured using an alamarBlue assay. Briefly, alamarBlue reagent was diluted 1:10 in complete Caco-2 medium to form a working solution, and the assay was run according to the manufacturer's instructions. Fluorescence values (Ex 560 nm, Em 590 nm) were normalized to acellular wells for TCP samples and to acellular constructs for SF and alginate. Caco-2 cell metabolic activities were assayed every 2–3 d for three weeks. The metabolic activity of InMyoFibs was also monitored using alamarBlue. Here, the alamarBlue reagent was diluted 1:10 in complete SmGM-2 to form the working solution, and fluorescence was measured on days 1, 3, 5, and 8.

To complement the alamarBlue assays and evaluate the potential cell damage to InMyoFibs that were subjected to the post-printing crosslinking, an LDH assay was performed on days 1, 3, 5, and 8 according to the manufacturer's instructions. Each day, the medium was extracted from the wells and placed into labelled microcentrifuge tubes and stored at −20 °C until all samples were collected. Absorbance was measured at 490 nm and 680 nm. Acellular wells and an LDH positive control (medium with 1% Triton X-100) were also assayed.

2.6.6. InMyoFib viability post-shearing

To determine the viability of the InMyoFibs post-printing, the cells were encapsulated in **SF-Ink** and sheared through a 27 G blunt needle to mimic printing conditions. The InMyoFibs were encapsulated via the two-step crosslinking method outlined in Section 2.5.4. Briefly, a 981 µl solution of 2%SF containing 1% gelatin and 0.02% fibronectin, 2.1 µl of 165 mM H_2O_2, and 10 µl of HRP was mixed with a cell suspension to obtain a final concentration of 5 million cells ml^{-1}. The cell density was increased to 5 million cells ml^{-1} to allow visualization of the cells, and subsequent quantification of viability. For the constructs that were not sheared, 0.1 ml of the **SF-Ink-2** was aliquoted via micropipette/pipette tip to a glass bottom dish. For sheared samples, 0.1 ml of the **SF-Ink-2** was delivered to a glass bottom dish using a syringe and a 27 G needle. Both sets of constructs were allowed to cure at 37 °C for 7 min, and then 50 µl of 1.30 mM H_2O_2 was added to complete crosslinking. The samples were cured for 20 min at 37 °C, the excess H_2O_2 was aspirated, and medium was added to the samples. The medium was replaced after 45 min and the samples were incubated overnight. Prior to imaging, 3 drops of NucBlue Live reagent and 3 drops of NucGreen Dead reagent (ReadyProbes Cell Viability Imaging Kit, ThermoFisher) were added to the medium of the samples, which were allowed to incubate for 3 h at 37 °C. A dead control (thermal treatment at 60 °C for 20 min) was used to assess staining. The cells were visualized using a Nikon A1 R spectral confocal microscope, and the cells were quantified via ImageJ (NIH, Bethesda, MD).

2.6.7. Statistical analysis

One-way ANOVA was run with a post-hoc Tukey test to evaluate the differences of the means. A statistically significant value was determined if the p-value was less than 0.05. Two-way ANOVA with a post-hoc Tukey test was used on final G' values for **SF-Ink-2** and **SF-Ink-4** prepared with water and PBS to evaluate the differences as a result of SF and salt concentrations. The same two-way ANOVA was carried out to assess any changes between Caco-2 cell attachment and proliferation on flat and topographic constructs that could be attributed to topography or SF concentration.

3. Results

3.1. Formulation of fully and partially crosslinked silk hydrogels

Scheme 1 shows the two different methods investigated to generate the printable SF hydrogels. SF hydrogel (**SF-Gel**) (Scheme 1, Method 1) formulations, prepared following the methods outlined in literature [26], contain sufficient HRP and hydrogen peroxide to result in an elastic hydrogel network. In contrast, reactive silk inks (**SF-Ink**) were prepared by reducing the volume of hydrogen peroxide added to the reacting SF solution. The result was a partially crosslinked solution (Scheme 1, Method 2(a)) that allowed for longer working times and enabled 3D printing of the reacting solution. **SF-Inks** were subjected to a post-processing crosslinking (Method 2(b)) and lock in the structure. Because the crosslinking process results in the formation of ditryosine bonds, the extent of the crosslinking reaction could be confirmed by measuring dityrosine bond fluorescence. The uncrosslinked SF solutions that lack ditryosine bonds display some fluorescence at these wavelengths, thus this fluorescence is not exclusive to the dityrosine bond. The **SF-Inks** displayed fluorescence in between that of uncrosslinked solutions and fully crosslinked **SF-Gels**, and the fluorescence was found to increase with increasing protein concentration (figure 1).

3.2. Rheological properties of SF hydrogels and SF inks

3.2.1. Oscillatory time sweeps

The effects of SF concentration, hydrogen peroxide concentration, and the inclusion of salts on shear storage modulus (G') and phase angle over time were monitored using oscillatory time sweeps. The results are shown in figure 2. Storage modulus always

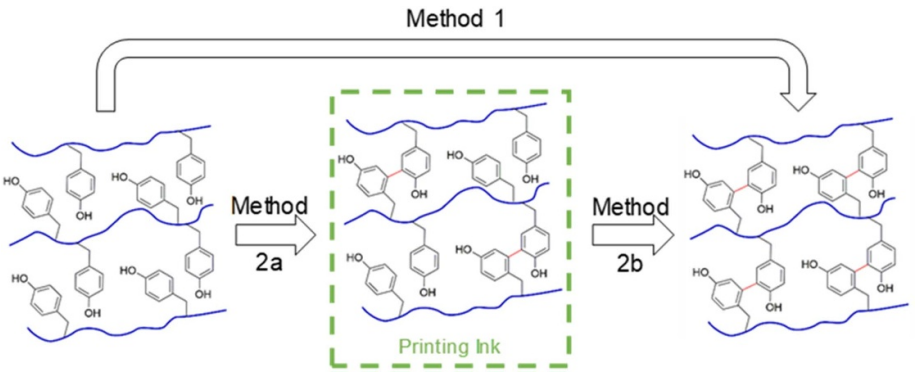

Scheme 1. Schematic of (**Method 1**) fully crosslinked silk hydrogel (**SF-Gel**) and (**Method 2**) partially crosslinked reactive ink silk hydrogels (**SF-Ink**).

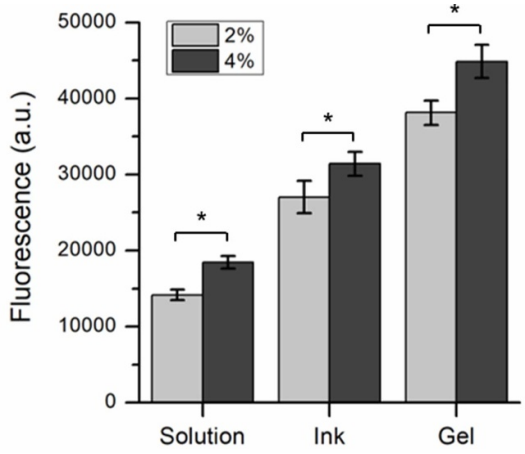

Figure 1. Fluorescence (Ex 315 nm, Em 400 nm) of dityrosine bonds in silk solutions, **SF-Inks**, and **SF-Gels**. * denotes significance at $p < 0.05$.

exceeded loss modulus for all formulations, even at the initial time points. Therefore, the onset of gelation was defined as the time when the phase angle ($\tan^{-1}$(G"/G')) started to decrease, and the gelation reaction was regarded as complete when the phase angle reached a quasi-static value. In SF hydrogels (**SF-Gel**) prepared with water (figure 2(a)), a reduction in SF concentration produced softer hydrogels, as indicated by decreased storage modulus values at the end of testing. In addition, reducing SF concentration increased the time required to complete gelation, which is most apparent in the gradual increase in moduli of the **SF-Gel-1** samples compared to the sharper increase observed around 900 s for the other concentrations. Reducing hydrogen peroxide concentration to formulate the **SF-Ink** reacting solutions caused the steady state storage modulus to decrease significantly (figure 2(b)). Because a decrease in hydrogen peroxide concentration leads to a decrease in crosslink density for this enzyme-mediated reaction, the resulting lower storage modulus values were expected. When hydrogen peroxide concentration is tailored for each tested SF concentration, partially crosslinked hydrogels (**SF-Inks**) of similar stiffness can be produced, as the storage modulus values were not found to be statistically different (figure 3).

The time sweeps also reveal that storage modulus of the **SF-Inks** plateaus more rapidly than **SF-Gels**. Though the **SF-Inks** rapidly reach a quasi-static value, they remain able to flow throughout the entire experimental time and thus display a much longer time to gelation than **SF-Gels**. This can be seen in the change of phase angle over time (figure 2(c)), where the phase angle reaches a quasi-static value earlier than for the corresponding SF hydrogels. This increased rate of gelation in the **SF-Inks** suggests that the HRP activity is enhanced with reduced hydrogen peroxide concentration. Studies examining the effect of hydrogen peroxide concentration on HRP activity have shown that HRP activity decreases and eventually can undergo inactivation with increasing hydrogen peroxide concentration [39, 40], which may explain the results observed here.

The addition of 10X PBS to the reacting solutions of both hydrogels and inks to prepare a 1X PBS solvent caused several rheological changes in the SF hydrogels and inks. The steady state storage modulus values for **SF-Gel-2** and **SF-Gel-4** were significantly lower than the corresponding water-only hydrogels and inks (figure 3). In **SF-Gel-4** with 1X PBS, the gelation rate at 37 °C (figure 2(d)) was similar to that of the **SF-Gel-4** with water at 25 °C (figure 2(a)). However, the addition of salt to the reacting SF solution for **SF-Gel-2** affected the gelation rate more noticeably, where the time to complete gelation was still slower at 37 °C than for the corresponding water-only hydrogel at 25 °C, as illustrated by the time to reach steady state in both storage modulus and phase angle values (figures 2(c), (f)). This data indicates that the addition of salt to the reacting solution affects gelation rate and reduces SF hydrogels stiffness, with these differences becoming larger for gels prepared at lower SF concentrations.

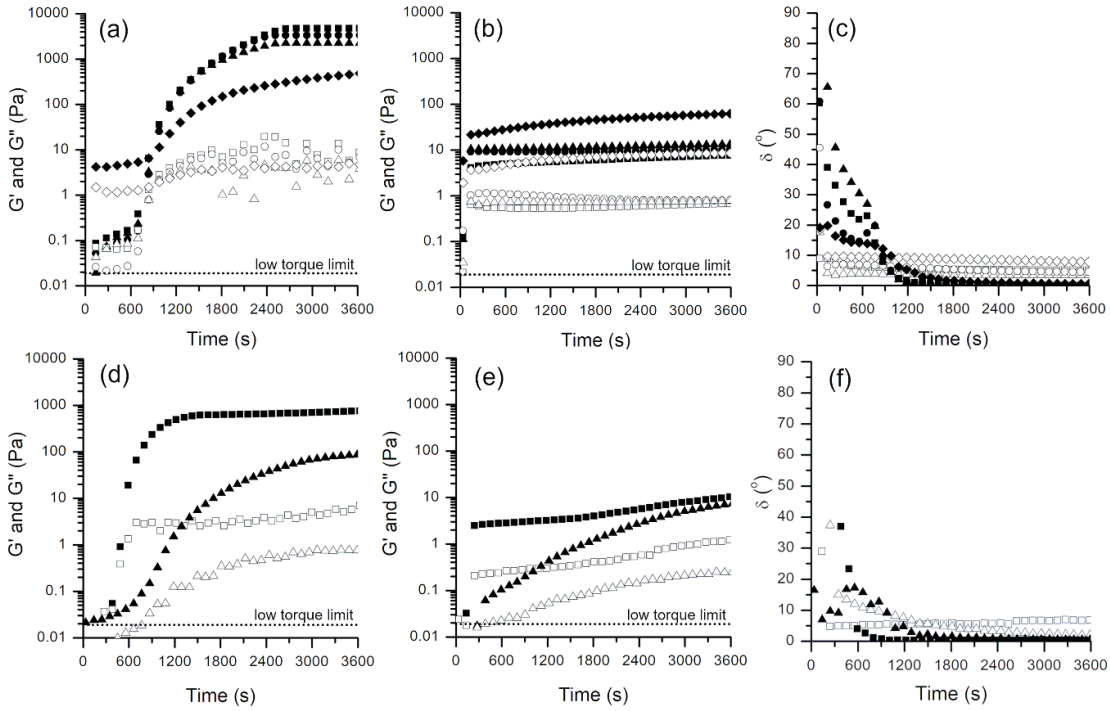

Figure 2. Oscillatory time sweeps showing storage (G') (closed symbols) and loss (G") (open symbols) of (a) fully crosslinked (**SF-Gel**) and (b) partially crosslinked (**SF-Ink**) SF hydrogels prepared in water at 25 °C. (c) Phase angle traces corresponding to the traces shown in (a), (b) for fully crosslinked (**SF-Gel**) (closed symbols) and partially crosslinked (**SF-Ink**) (open symbols). Oscillatory time sweeps showing storage (G') (closed symbols) and loss (G") (open symbols) of (d) fully crosslinked (**SF-Gel**) and (e) partially crosslinked (**SF-Ink**) SF hydrogels prepared in 1X PBS at 37 °C. (f) Phase angle traces corresponding to the traces shown in (d), (e) for fully crosslinked (**SF-Gel**) (closed symbols) and partially crosslinked (**SF-Ink**) (open symbols). For all plots, the following SF concentrations apply: 4% (square), 3% (circle), 2% (triangle), and 1% (diamond).

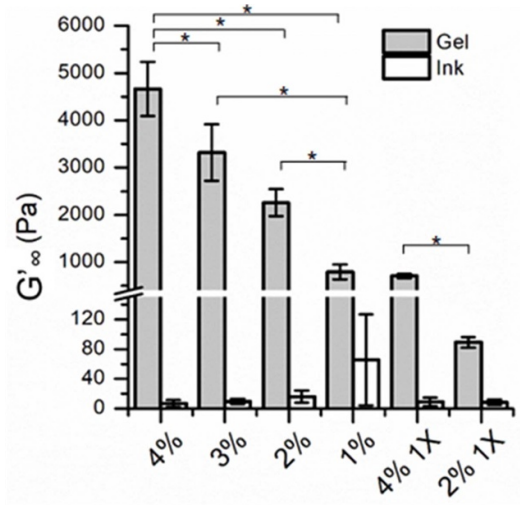

Figure 3. Average G' values after gelation for **SF-Gel** and **SF-Ink** formulations with varying SF concentrations and different salt concentrations after curing for 1 h at 37 °C. (n = 3, bars note standard deviation, *denotes $p < 0.05$).

Similar to the water-only SF inks, the reduction of hydrogen peroxide to the reacting 1X PBS **SF-Inks** (figures 2(e), (f)) showed an increased rate of gelation compared to the 1X PBS **SF-Gels** (figures 2(d), (f)). Again, this could be attributed to the enhanced enzymatic activity of HRP [39, 40]. Interestingly, the average storage modulus values at the end of the 1 h testing period were similar to those of the corresponding SF inks prepared in water (figure 3). Two-way ANOVA showed no statistical significance between the **SF-Ink-4** and **SF-Ink-2** prepared with either water or 1X PBS. The rate of gelation for these two 4% SF inks were also similar (figures 2(b) and (e)). Like the 2% SF hydrogels, however, **SF-Ink-2** appeared to be more notably affected by the 1X PBS. This can be observed by the drastic reduction on gelation rate (figure 2(f)) where the phase angle reaches steady state at approximately 2400 s. In comparison, the phase angles of **SF-Ink-4** with 1X PBS and **SF-Ink-2** with water achieved steady state at roughly 250 s and 100 s, respectively.

3.2.2. Oscillatory frequency sweeps

The frequency-dependent behaviour of SF hydrogels and inks was assessed using oscillatory frequency sweeps (figure 4). These experiments were carried out after the oscillatory time sweeps were completed so that the samples had already reached constant storage modulus and phase angle values. All compositions show shear thinning behaviour, however the magnitude of the complex viscosity is smaller for **SF-Inks** than for **SF-Gels**. These results suggests that the **SF-Inks** are more printable from the perspective that lower pressures are required to eject the **SF-Inks** from the printing nozzle compared to the **SF-Gels**.

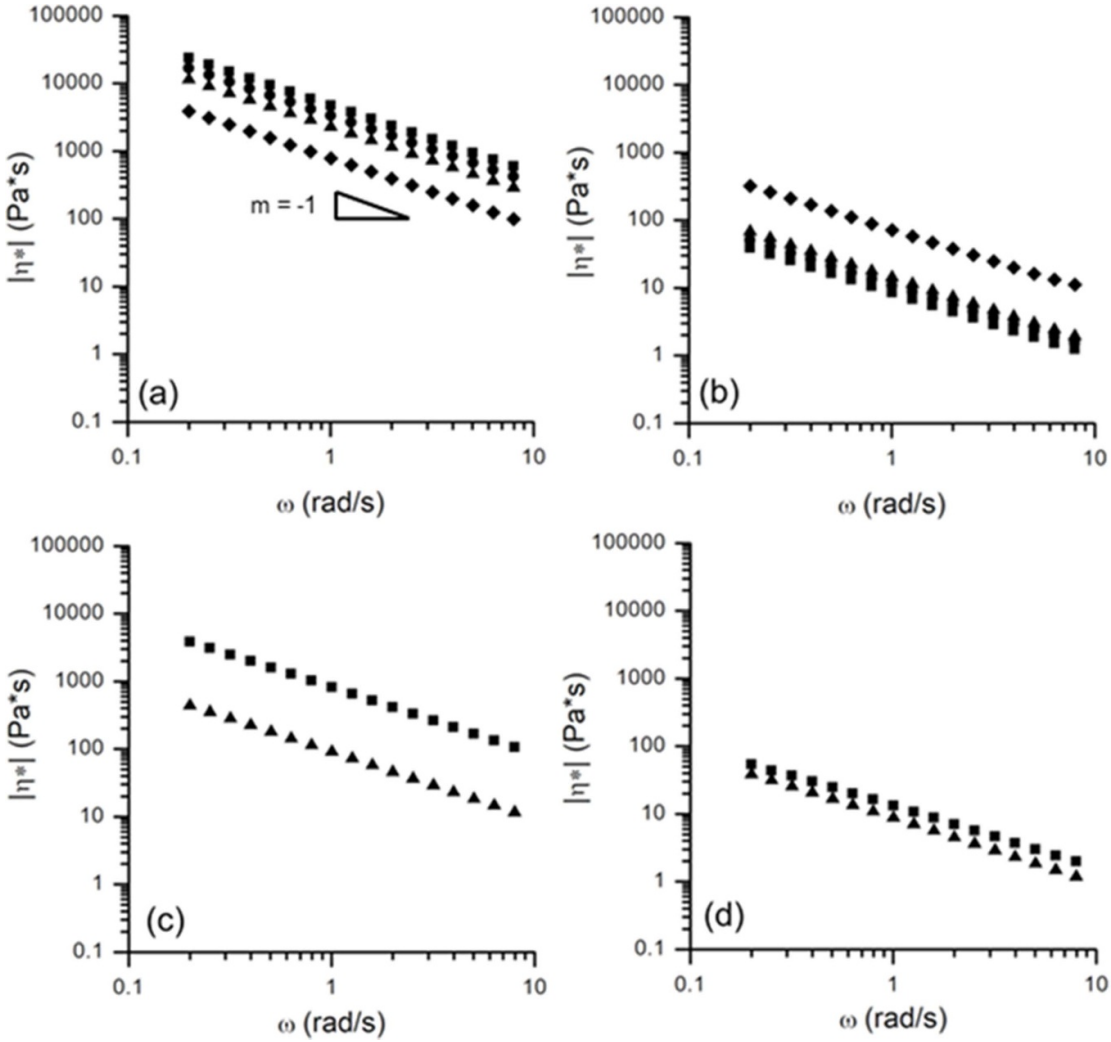

Figure 4. Complex viscosity measured from oscillatory frequency sweeps of (a) fully crosslinked (**SF-Gel**) hydrogels prepared in water at 25 °C, (b) partially crosslinked (**SF-Ink**) hydrogels prepared in water at 25 °C, (c) fully crosslinked (**SF-Gel**) hydrogels prepared in 1X PBS at 37 °C, and (d) partially crosslinked (**SF-Ink**) hydrogels prepared in 1X PBS at 37 °C. The SF concentrations shown are 4% (square), 3% (circle), 2% (triangle), and 1% (diamond)).

The exchange of water for PBS as the solvent did not appear to significantly affect the viscoelastic properties of the SF hydrogels and inks. The **SF-Gels** (figure 4(c)) and **SF-Inks** (figure 4(d)) in 1X PBS again showed shear thinning behavior throughout the frequency range for all tested concentrations, with the **SF-Inks** having lower complex viscosity than the **SF-Gels**. The SF-Ink showed a higher degree of shear thinning compared to alginate solutions with similar concentrations [41]. During printing, a high degree of shear thinning implies that a lower viscosity will be attained upon shear and a smaller pressure will be required for printing. As the ink exits the nozzle and the shear rate quickly diminishes, highly shear thinning inks will maintain the shape of the as-printed structures better [42]. In addition to require less pressure applied during printing, **SF-Inks** are also more desirable for printing because **SF-Gels** continue to crosslink over time, which not only can broaden the range in viscosities encountered during printing but may also pose a risk for clogging of the printing needle.

3.3. 3D printing of SF-inks with water

3.3.1. Effect of H_2O_2 concentration on SF-ink structure after printing

The printability of the **SF-Inks** with water were examined visually in conjunction with rheological testing. In figure 5, **SF-Ink-4** with varying final concentrations of H_2O_2 were extruded using a Hyrel System 30 M printer through a 27 G blunt needle. When no hydrogen peroxide was added to the ink solution, the ink was extruded as a droplet (figure 5(a)). The addition of 272 μM H_2O_2 still resulted in a droplet upon extrusion (figure 5(b)). Upon further addition of H_2O_2 to 289 μM, a filament of **SF-Ink-4** was produced instead of a droplet (figure 5(c)). Droplet formation indicates the relative importance the between viscosity and surface tension and has implications on printability of the inks. If surface tension is relatively

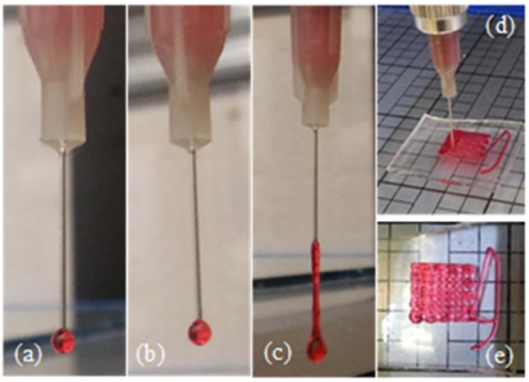

Figure 5. Images of (a) 4% silk solution, (b) **SF-Ink-4** containing 272 μM H_2O_2, and (c) **SF-Ink-4** containing 289 μM H_2O_2 deposited through a 27 G blunt needle. (d) Printing of a construct using **SF-Ink-4** containing 289 μM H_2O_2, and (e) a completed 2-layer construct printed from the **SF-Ink-4** containing 289 μM H_2O_2. All silk solutions in this image contained red food dye (FD&C Red 40 and 3) to assist in visualization.

high compared to viscosity, droplets are expected to form. Therefore, droplet formation could be an indication of a relatively low viscosity of the extrudate, which is more prone to collapse as additional layers are printed on top. Additionally, if surface tension or contact angle with the surface is too high, printed lines will dewet to form drops instead of continuous printed lines.

Printability of the inks was also assessed by printing a two-layer construct (figures 5(d)–(e)). A two-layer construct of **SF-Ink-4** in water was printed and subsequently crosslinked with adequate hydrogen peroxide to achieve the shape shown in figure 5(e). The structure was visually examined for evidence of collapse of the printed structure, but this was not observed. This supports the rheological evidence that the SF solutions, when crosslinked into a **SF-Ink** using hydrogen peroxide concentrations described in the methods section, result in the extrusion of a filament rather than a droplet and are suitable for 3D printing.

3.3.2. FTIR of sheared and non-sheared SF solutions and inks

SF solutions and SF Inks in water and in PBS were prepared as described above and then either cast directly into a hydrogel or sheared through the 27 G blunt needle used for printing prior to casting. The deposited materials were dried at room temperature and subsequently characterized using ATR-FTIR to assess secondary structures in the amide I region of the spectra. It was expected that passing the **SF-Inks** through the printing needle could promote in beta sheet formation due to the shearing of the ink. Further, it was expected that the beta sheet content would be higher in **SF-Inks** compared to SF solutions because of **SF-Inks** have a higher viscosity. Non-sheared samples for both SF solutions (figure 6(a)) and inks (figure 6(b)) prepared in water did not show noticeable peaks characteristic to beta-sheets, as expected. Upon shearing, SF solutions also did not exhibit beta-sheet peaks in the FTIR spectrum (figure 6(a)). However, each of the SF ink formulations showed a shift and evolution of peaks in the range between 1616–1637 cm^{-1}, demonstrating that the increase in viscosity facilitated the formation of beta-sheets in the printed material [38]. The FTIR spectra were deconvoluted [38] and the average beta sheet content for silk solutions and inks with and without shearing are shown in Fig. S1. The beta sheet content was significantly higher for sheared inks than for inks that were not sheared, but beta sheet content did not increase when solutions that lacked HRP and H_2O_2 were sheared, suggesting there exists a threshold shear stress above which beta-sheet formation[43] is induced by shear.

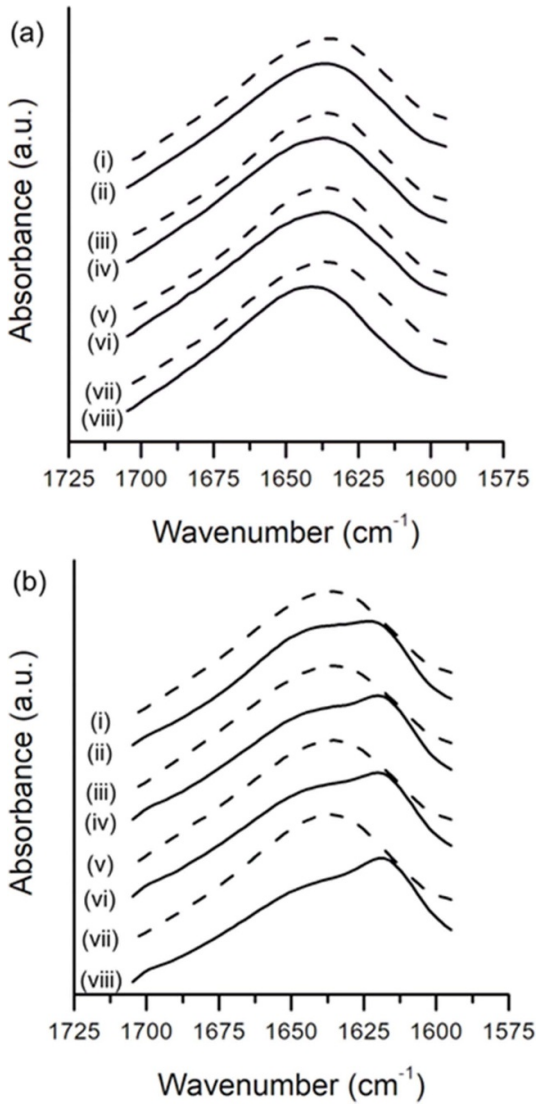

Figure 6. ATR-FTIR spectra of sheared and non-sheared (a) SF solutions and (b) SF inks prepared in water. For each plot, (i): 4% not sheared; (ii): 4% sheared; (iii): 3% not sheared; (iv): 3% sheared; (v): 2% not sheared; (vi): 2% sheared; (vii): 1% not sheared; (viii): 1% sheared.

3.3.3. Effect of post-printing processing on programmed hole diameters

Printed constructs with varying **SF-Inks** and programmed hole diameters were imaged to examine the effects of post-printing processing on the hole diameters and how the hole diameters compared to the original programmed hole diameter. The microscope images are shown in figure 7. **SF-Ink-2, SF-Ink-3**, and **SF-Ink-4** were characterized because printed **SF-Ink-1** constructs were too fragile to handle after crosslinking. Images were taken after printing, after crosslinking, and after sterilization with 70% EtOH. After each step and before imaging, samples were equilibrated with dH_2O to reach equilibrium water content and shape. Hole diameters were designed to be approximately 1000 μm. After printing, the hole diameters of the constructs were calculated to be approximately 650–700 μm for all concentrations tested. A dimensionless flow rate[44], *Qr*, was calculated using the nozzle's diameter, the size of the gap between the nozzle and substrate, the translation speed of the nozzle, and the volumetric flow rate of silk that was determined experimentally using mass flow rate and density at varying protein concentrations. It was found that the ink was slightly over-extruded, where Qr valued at 2.75 for 4% silks and 4.5 for 2% silks, which contributes to the observed hole size being smaller than the programmed hole size. This indicates that additional ink may have been extruded during printing and/or gravity-induced spreading of the printed line. The most notable impact on hole diameter overall occurred after sterilization, where hole diameters decreased significantly compared to those of the as-printed and crosslinked sample regardless of SF concentration. This was attributed to ethanol inducing beta-sheets, causing a decrease in overall size of the construct and holes as a result. Sterilization by filtering solutions prior to printing could abrogate this shape change by eliminating the need for ethanol treatment, but this was not investigated in this work.

Programmed hole sizes were varied in printed **SF-Ink-3** constructs to examine the effect of post-printing processing on the final hole diameters (figure S2). The same trend in average hole diameters that was found when varying SF concentration occurred here as well, where the major impact on average hole diameter arose after sterilization for all programmed hole sizes. Additionally, the final average hole diameters were calculated to be approximately 50% of the original programmed size, similar to the results found when varying SF concentration. Notably, a threshold hole diameter seems to be present, where below this threshold produces constructs with a hydrogel layer on the bottom. The construct printed with a programmed hole diameter of 1200 μm does not have a bottom hydrogel layer after sterilization. Once the programmed hole diameter is decreased to 1000 μm,

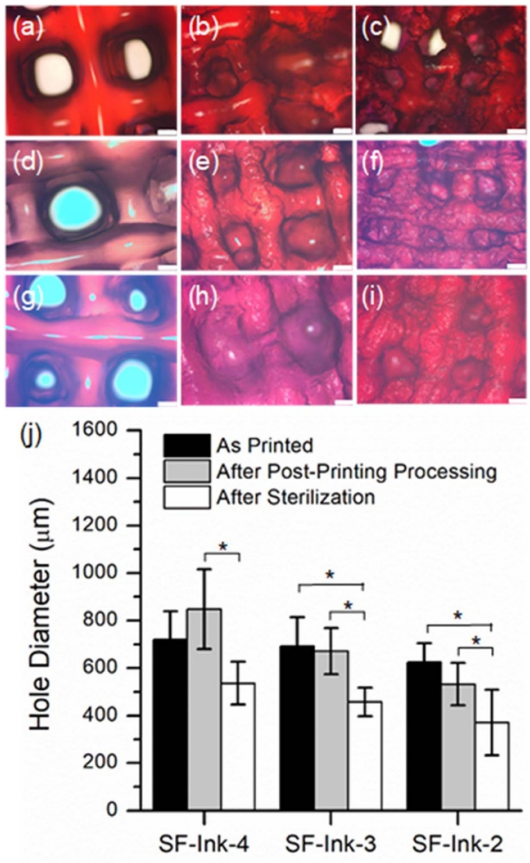

Figure 7. (a)–(i) Optical microscope images of printed **SF-Ink** constructs using varying silk concentrations. Silk concentrations of (a)–(c) **SF-Ink-2**, (d)–(f) **SF-Ink-3**, and (g)–(i) **SF-Ink-4** were selected to examine hole width after printing (a), (d), (g), after post-printing processing (b), (e), (h), and after sterilization (c), (f), (i). (j) Averages and standard deviations for each hole width and processing step were calculated and one-way ANOVA was used to test for statistical significance (a * denotes $p \leq 0.05$). Scale bars denote 200 μm.

however, this layer appears after crosslinking. This threshold may change when protein concentration is changed, though this was not investigated in this work. Importantly, changes in the dimensions of the holes are predictable so it is possible to design constructs with a final shape by accounting for the change in the AutoCAD design. Additionally, changes in the dimensions of the holes may be avoided in the future by sterilizing the silk prior to printing (i.e. by autoclaving or sterile filtering) and printing sterile constructs.

3.3.4. Stability of constructs over time

Silk-Ink-3 was printed into a 1 cm × 1 cm construct with an overall thickness of approximately 1.2 mm, as designed in AutoCAD. The constructs were subjected to post-printing processing and sterilization according to the methods described above. Acellular constructs were incubated in sterile medium at 37 °C at 5% CO_2 and periodically removed from the incubator, imaged using a stereo microscope and optical microscope (sterility

maintained during imaging), and the sizes of the holes were quantified using image analysis with ImageJ (Fig. S3). No statistically significant change in the overall dimensions of the construct or in the size of the holes was observed over a period of nine weeks. Any change in shape that occurs in acellular constructs thus occurs immediately, and the constructs have the potential to serve as culture substrates with longer term stability than collagen constructs.

3.3.5. Effect of SF concentration on average depth of holes in printed constructs

Confocal microscopy and ImageJ were used to calculate the average depths of the crypt-like structures in printed **SF-Ink-4** and **SF-Ink-2** constructs (figure 8). These SF concentrations were selected for this study and for cell culture experiments because of the significant differences found in the rheological data. The crypt-like structures of both the printed **SF-Ink-4** and **SF-Ink-2** samples show similar depths. However, because the average hole sizes for the **SF-Ink-4** constructs are larger than those of the **SF-Ink-2** constructs, the crypt-like structures of the **SF-Ink-4** constructs exhibit a larger radius of curvature compared to the **SF-Ink-2** constructs. Average depths were calculated for three samples at each concentration and showed no statistical significance between hole sizes of the same SF concentration, indicating reproducibility, or between SF concentrations, suggesting that SF concentration does not play a role in determining hole depth. The dimensions of the constructs used in this experiment (1 cm × 1 cm with a target thickness of 1.2 mm as designed in AutoCAD) were used in subsequent cell culture experiments. **Alg-Ink-3** constructs were also printed using these dimensions. Additionally, because the presence of crypt-like structures in the SF constructs alters the surface area, as described in the methods section, the surface area was taken into consideration for Caco-2 seeding onto these substrates.

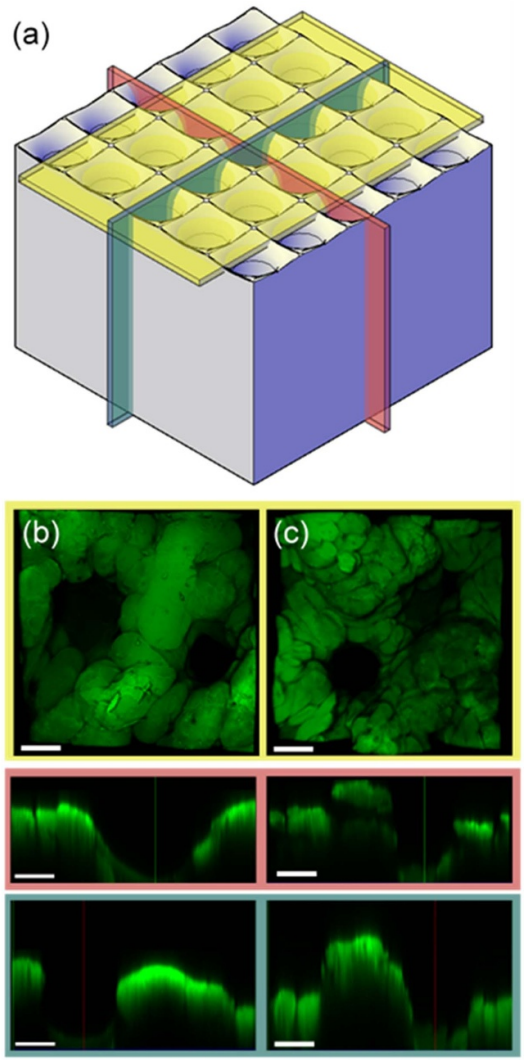

Figure 8. (a) Schematic of construct with image planes highlighted (the schematic is not drawn to scale). Confocal microscope images and z-stacks of printed (b) **SF-Ink-4** and (c) **SF-Ink-2** silk constructs printed from water solutions and dyed with DAPI. The scale bar represents 200 μm.

3.4. Cell culture

3.4.1. Attachment of Caco-2 cells onto flat and crypt-like constructs

The effects of SF concentration and topography on Caco-2 attachment were studied and compared to Caco-2 attachment onto TCP and printed alginate. Because both silk and alginate lack integrin binding sites, a fibronectin (FBN) and gelatin solution was used to facilitate cell attachment. An alamarBlue assay was used on day 1 to calculate cell attachment using a standard curve. The results are shown in figure 9(a). No statistically significant difference in cell attachment was found for Caco-2 cell attachment on hydrogels of different stiffness (through protein concentration) or on hydrogels of different topography (flat or crypt-like).

3.4.2. Caco-2 proliferation and morphology

Proliferation of Caco-2 cells seeded onto flat and crypt-like printed **SF-Ink** constructs, **Alg-Ink-3** constructs, or TCP was monitored over a 19-d period using cell metabolic activity measured by alamarBlue. Over the testing period, relative fluorescence increased for all samples in general (figure 9(b)), which was taken as an increase in cell proliferation. No statistically significant differences in proliferation for cells grown on the **SF-Ink** constructs with regards to topography and SF concentration were found. This suggests that SF concentration does not affect Caco-2 proliferation, and the topography achieved through the 3D printing process used does not produce a change in Caco-2 proliferation as well. The proliferation for TCP was slower than that of the SF constructs, which could be attributed to the higher cell attachment leading to contact inhibition for cells grown on TCP. Caco-2 cells grown on flat

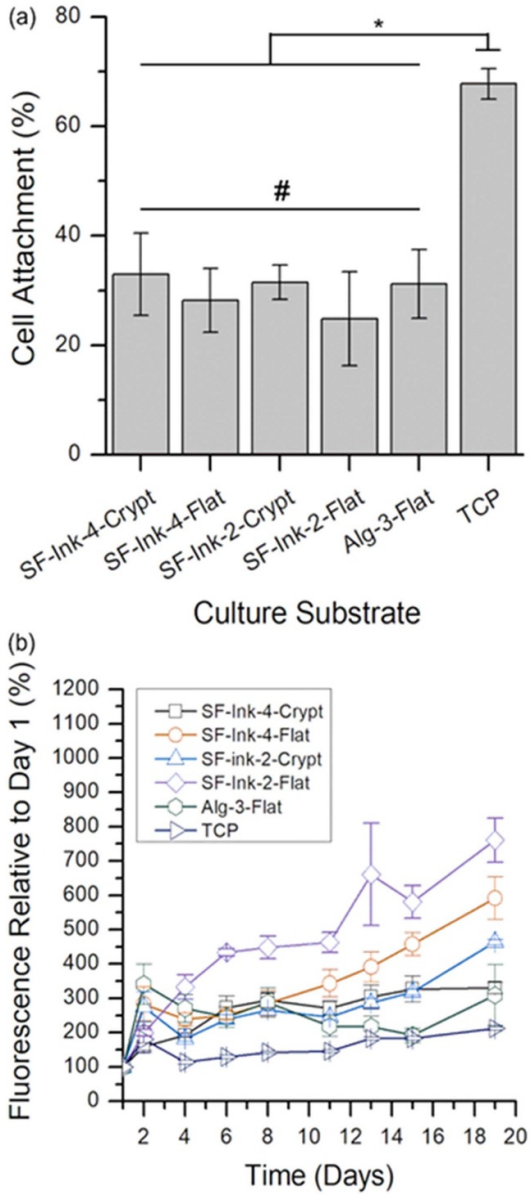

Figure 9. (a) Caco-2 attachment onto printed SF and alginate hydrogels and TCP, as calculated by alamarBlue. (b) Proliferation of Caco-2 cells grown on TCP (right triangle), **Alg-Ink-3-Flat** (hexagon), **SF-Ink-4-Flat** (circle), **SF-Ink-4-Crypt** (square), **SF-Ink-2-Flat** (diamond), and **SF-Ink-2-Crypt** (upward triangle). Error bars represent standard deviation, * denotes a p-value less than 0.05, and # denotes lack of significance at a p-value less than 0.05.

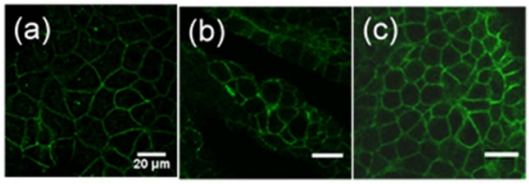

Figure 10. Claudin-1 staining highlighting tight junction formation by Caco-2 cells on (a) TCP, (b) **SF-Ink-4-Crypt**, and (c) **SF-Ink-4-Flat**. Scale bars represent 20 μm.

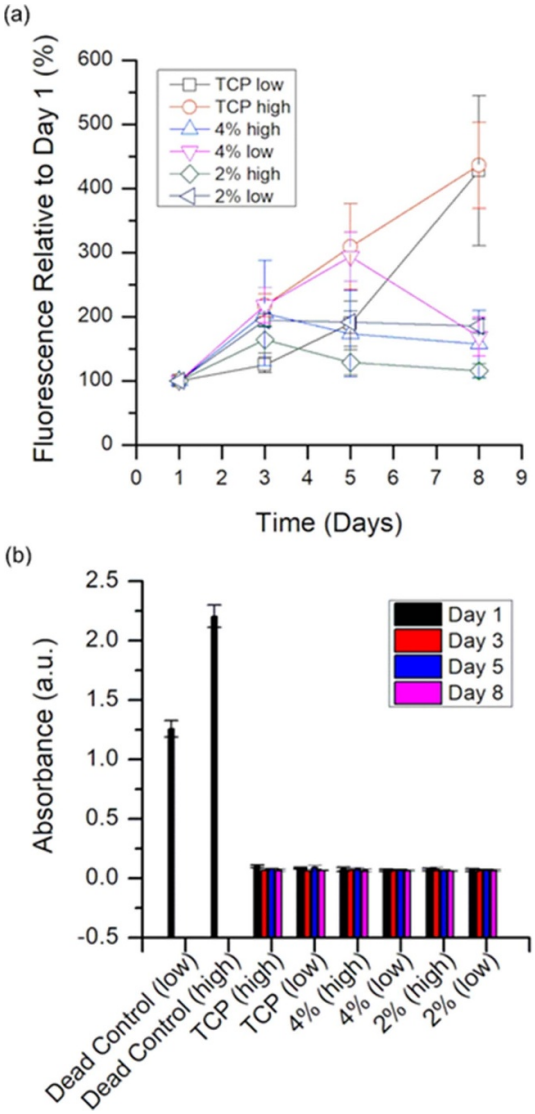

Figure 11. (a) InMyoFib metabolic activity on TCP and encapsulated within **SF-Ink-4** and **Silk-Ink-2** gels. (b) LDH content in cell culture supernatants. The dead control is medium containing 1% Triton X-100. For TCP, the low density corresponds 10 000 cells well^{-1} and the high density corresponds to 38 000 cells well^{-1}. For hydrogels, the low density corresponds 100 000 cells well^{-1} and the high density corresponds to 380 000 cells well^{-1}.

Alg-Ink-3 constructs decreased after day 8, which was attributed to dissolution/breakup of the alginate construct. With regards to the printed flat and crypt-like **SF-Ink** constructs, statistical significance of proliferation varied with respect to TCP. Despite this variation, proliferation of Caco-2 cells on SF constructs was in general greater than that of Caco-2 cells grown on TCP and was anticipated to be due to more surface area available for the cells to grow on the hydrogel constructs compared to the TCP, where initial attachment was higher.

Confocal imaging of Caco-2 cells onto printed flat and crypt-like SF constructs, printed flat alginate, and TCP was used to examine changes in morphology weekly over a 28-d period (Fig. S4). Z-stacks were obtained as well to assess any changes in cell morphology with regards to topography. Images taken on day 1 showed greater attachment of Caco-2 cells on

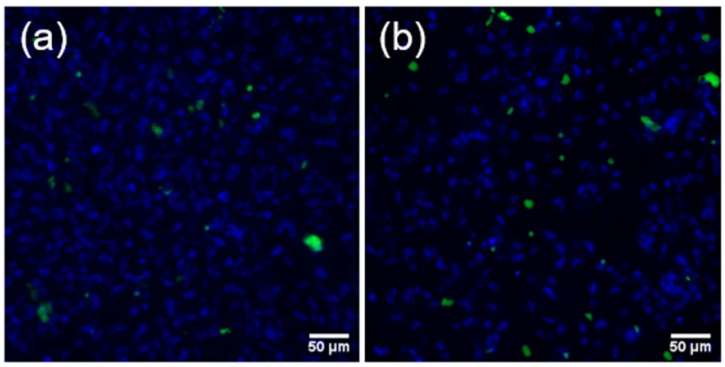

Figure 12. Images of InMyoFibs encapsulated in (a) non-sheared **SF-Ink-2** and (b) sheared **SF-Ink-2**. Blue staining indicates nuclei of all cells, while green stains indicate nuclei of dead cells.

the glass-bottom dish than on SF and alginate constructs, in agreement with the cell attachment data shown in figure 9(a). Cells grown on all samples on day 1 also exhibited a rounded/globular morphology. Cells seeded onto topographic SF constructs were also found primarily at the bottom of the 'crypts'. On day 8, cells grown on glass-bottom dishes reached confluence and adopted a 'cobblestone' morphology, whereas cells grown on SF and alginate constructs showed an increase in cell coverage, but the cells were still subconfluent and appeared to maintain a rounded/globular morphology. Upon day 15, the cells seeded onto SF and alginate constructs appeared to have reached confluence and remained as an intact layer through the experiment's duration (minimum 28 d). The ability of the Caco-2 cells to form tight junctions on different topographies was also evaluated after 28 d of culture, as shown in figure 10. Cells seeded on the constructs or TCP were fixed using ice cold methanol for 5 min before staining with claudin-1 antibody (1:50 dilution in 1X PBS). It was observed that for tight junctions formed on TCP (figure 10(a)), **SF-Ink-4-Crypt** (figure 10(b)), and **SF-Ink-4-Flat** (figure 10(c)), and that the ability of Caco-2 cells to form tight junctions was not affected by the topography of the constructs or the post-printing treatment with H_2O_2.

3.4.3. Encapsulated InMyoFib proliferation

InMyoFibs were encapsulated in **SF-Ink-4** and **SF-Ink-2** hydrogels and proliferation was measured over time and compared to InMyoFib grown on TCP. As described in the Experimental Section, the size of the TCP well was selected so that number of cells plated on TCP matched the number of cells encapsulated within the gels. Additionally, the reacting SF solutions contained 1X PBS instead of water to maintain osmolarity. The effects of cell density and SF concentrations on proliferation were measured using alamarBlue (figure 11(a)). Specifically, cells were plated on TCP at either 10 000 cells well^{-1} (low density) or 38 000 cells well^{-1} (high density), and encapsulated in gels at either 100 000 cells ml^{-1} (low density) or 380 000 cells ml^{-1} (high density). Both TCP cell densities were found to proliferate consistently over the experimental period. In contrast, **SF-Ink-2** and **SF-Ink-4** at both densities increased in relative fluorescence until day 5, after which the relative fluorescence values started to decrease towards day 1 values. These trends were found to be reproducible, though the peak of the fluorescence could be pushed to later in the culture by encapsulating at an initially lower cell density.

Because of this decrease in cell metabolic activity during culture, an LDH assay was run in parallel on the culture supernatants to assay for cell damage. LDH levels were no different as a function of time in culture (figure 11(b), indicating that the cells are likely becoming less proliferative rather than dying in the culture. Because SF is still the major component of the hydrogel (fibronectin and gelatin are minor components) and because SF does not degrade over this time period in culture, this slowing of metabolic activity and proliferation is reasonable. Increasing the ratio of FBN/gelatin relative to silk fibroin may promote expansion of InMyoFib further, but this was not the focus of this study.

The viability of encapsulated InMyoFibs was investigated to determine the potential of bioprinting the constructs. The InMyoFibs were encapsulated in **SF-Ink-2** hydrogels and were dispensed by micropipette/pipette tip (non-sheared) and syringe/needle (sheared). The cells were stained with ReadyProbes Cell Viability Imaging Kit (Blue/Green), imaged with confocal microscopy (figure 12), and the viability was determined. This kit stains nuclei of all cells blue and nuclei of cells with compromised plasma membrane integrity (dead cells) green. Imaging of a dead control (sample heated to 60 °C for 20 min) was performed to ensure expected staining results and is shown in Fig. S5. For the non-sheared samples, the average viability was 92%, while the sheared samples exhibited a viability of about 87%. The relatively high viability of the sheared samples

indicates that the shearing does not affect cell survivability.

4. Conclusions

This work presents a new reactive silk ink formulation designed for extrusion 3D printing of protein-based hydrogels at room temperature. The reactive silk inks use enzyme-catalyzed dityrosine bond formation to increase the protein solution's viscosity, thereby generating an ink with appropriate rheology for 3D printing. Tailoring the peroxide concentration the reactive ink enables the silk to be extruded as a filament and printed into hydrogel constructs, supporting successive printed layers without flow of the construct or loss of desired geometry. Compared to alginate hydrogels, acellular 3D printed silk hydrogels display superior shape retention, maintaining their printed shape when maintained in culture medium for at least nine weeks, a finding that is expected to enable investigation of longer-term cultures. Caco-2 attachment, proliferation, and tight junction formation was not found to be affected by the geometry of the constructs tested or post-printing processing. Shearing the reactive inks did not reduce the viability of encapsulated InMyoFibs significantly, and encapsulated myofibroblasts were found to proliferate over a period of 8 d before reaching a steady state level of metabolic activity within the hydrogel constructs. The work here thus provides a suitable route for extrusion 3D printing of protein hydrogel constructs that maintain their shape during printing and culture, without the need to vary temperature during printing or add additional components, such as synthetic polymers or inorganic materials.

Acknowledgments

The authors wish to thank Connecticut Innovations for funding through the Connecticut Regenerative Medicine Fund (15-RMA-UCONN-02). The authors also wish to thank the University of Connecticut for supporting this work through laboratory start-up funds and a Summer Undergraduate Research Fund (SURF) Award to support the work of Marisa Boch. The authors woud finally like to acknowledge Dr Christopher O'Connell for microscopy advice and assistance in obtaining the confocal images, which were acquired using a Leica SP8 microscope obtained through an award from the National Institutes of Health (NIH S10OD016435).

ORCID iDs

Anson W K Ma https://orcid.org/0000-0002-2865-5776
Kelly A Burke https://orcid.org/0000-0002-6741-0114

References

[1] DebRoy T, Wei H L, Zuback J S, Mukherjee T, Elmer J W, Milewski J O, Beese A M, Wilson-Heid A, De A and Zhang W 2018 Additive manufacturing of metallic components – process, structure and properties *Prog. Mater. Sci.* **92** 112–224
[2] Frazier W E 2014 Metal additive manufacturing: A review *J. Mater. Eng. Perform.* **23** 1917–28
[3] Gmeiner R, Deisinger U, Schönherr J, Lechner B, Detsch R, Boccaccini A R and Stampfl J 2015 Additive manufacturing of bioactive glasses and silicate bioceramics *J. Ceram. Sci. Technol.* **6** 75–86
[4] Ngo T D, Kashani A, Imbalzano G, Nguyen K T Q and Hui D 2018 Additive manufacturing (3D printing): A review of materials, methods, applications and challenges *Composites* B **143** 172–96
[5] Wang X, Jiang M, Zhou Z, Gou J and Hui D 2017 3D printing of polymer matrix composites: A review and prospective *Composites* B **110** 442–58
[6] Truby R L and Lewis J A 2016 Printing soft matter in three dimensions *Nature* **540** 371–8
[7] Ligon S C, Liska R, Stampfl J, Gurr M and Mülhaupt R 2017 Polymers for 3D printing and customized additive manufacturing *Chem. Rev.* **117** 10212–90
[8] DesRochers T M, Suter L, Roth A and Kaplan D L 2013 Bioengineered 3D human kidney tissue, a platform for the determination of nephrotoxicity *PLoS ONE* **8**
[9] Duval K, Grover H, Han L-H, Mou Y, Pegoraro A F, Fredberg J and Chen Z 2017 Modeling physiological events in 2D vs. 3D cell culture *Physiology* **32** 266–77
[10] Tavana H, Mosadegh B and Takayama S 2010 Polymeric aqueous biphasic systems for non-contact cell printing on cells: engineering heterocellular embryonic stem cell niches *Adv. Mater.* **22** 2628–31
[11] Chung J H Y, Naficy S, Yue Z, Kapsa R, Quigley A, Moulton S E and Wallace G G 2013 Bio-ink properties and printability for extrusion printing living cells *Biomater. Sci.* **1** 763–73
[12] Ozbolat I T and Hospodiuk M 2016 Current advances and future perspectives in extrusion-based bioprinting *Biomaterials* **76** 321–43
[13] Hinton T J, Jallerat Q, Palchesko R N, Park J H, Grodzicki M S, Shue H-J, Ramadan M H, Hudson A R and Feinberg A W 2015 Three-dimensional printing of complex biological structures by freeform reversible embedding of suspended hydrogels *Sci. Adv.* **1** e1500758
[14] Jin Y, Liu C, Chai W, Compaan A and Huang Y 2017 Self-supporting nanoclay as internal scaffold material for direct printing of soft hydrogel composite structures in air *ACS Appl. Mater. Interfaces* **9** 17456–65
[15] Ahlfeld T, Cidonio G, Kilian D, Duin S, Akkineni A R, Dawson J I, Yang S, Lode A, Oreffo R O C and Gelinsky M 2017 Development of a clay based bioink for 3D cell printing for skeletal application *Biofabrication* **9** 034103
[16] Peak C W, Stein J, Gold K A and Gaharwar A K 2018 Nanoengineered colloidal inks for 3D bioprinting *Langmuir* **34** 917–25
[17] Rodriguez M J, Brown J, Giordano J, Lin S J, Omenetto F G and Kaplan D L 2017 Silk based bioinks for soft tissue reconstruction using 3-dimensional (3D) printing with in vitro and in vivo assessments *Biomaterials* **117** 105–15
[18] Hoch E, Schuh C, Hirth T, Tovar G E M and Borchers K 2012 Stiff gelatin hydrogels can be photo-chemically synthesized from low viscous gelatin solutions using molecularly functionalized gelatin with a high degree of methacrylation *J. Mater. Sci. Mater. Med.* **23** 2607–17
[19] Hoch E, Hirth T, Tovar G E M and Borchers K 2013 Chemical tailoring of gelatin to adjust its chemical and physical properties for functional bioprinting *J. Mater. Chem.* B **1** 5675–85
[20] Du M, Chen B, Meng Q, Liu S, Zheng X, Zhang C, Wang H, Li H, Wang N and Dai J 2015 3D bioprinting of BMSC-laden

methacrylamide gelatin scaffolds with CBD-BMP2-collagen microfibers *Biofabrication* **7** 044104
[21] Akkineni A R, Ahlfeld T, Lode A and Gelinsky M 2016 A versatile method for combining different biopolymers in a core/shell fashion by 3D plotting to achieve mechanically robust constructs *Biofabrication* **8** 045001
[22] Xu T, Gregory C A, Molnar P, Cui X, Jalota S, Bhaduri S B and Boland T 2006 Viability and electrophysiology of neural cell structures generated by the inkjet printing method *Biomaterials* **27** 3580–8
[23] Schense J C and Hubbell J A 1999 Cross-linking exogenous bifunctional peptides into fibrin gels with factor XIIIa *Bioconjug. Chem.* **10** 75–81
[24] Wang X, Yan Y and Zhang R 2010 Recent trends and challenges in complex organ manufacturing *Tissue Eng. Part B* **16** 189–97
[25] Rockwood D N, Preda R C, Yucel T, Wang X, Lovett M L and Kaplan D L 2011 Materials fabrication from *Bombyx mori* silk fibroin *Nat. Protoc.* **6** 1612–31
[26] Partlow B P, Hanna C W, Rnjak-Kovacina J, Moreau J E, Applegate M B, Burke K A, Marelli B, Mitropoulos A N, Omenetto F G and Kaplan D L 2014 Highly tunable elastomeric silk biomaterials *Adv. Funct. Mater.* **24** 4615–24
[27] Kim S H *et al* 2018 Precisely printable and biocompatible silk fibroin bioink for digital light processing 3D printing *Nat. Commun.* **9** 1620
[28] Compaan A M, Christensen K and Huang Y 2017 Inkjet bioprinting of 3D silk fibroin cellular constructs using sacrificial alginate *ACS Biomater. Sci. Eng.* **3** 1519–26
[29] Huang L, Du X, Fan S, Yang G, Shao H, Li D, Cao C, Zhu Y, Zhu M and Zhang Y 2019 Bacterial cellulose nanofibers promote stress and fidelity of 3D-printed silk based hydrogel scaffold with hierarchical pores *Carbohydr. Polym.* **221** 146–56
[30] Das S, Pati F, Chameettachal S, Pahwa S, Ray A R, Dhara S and Ghosh S 2013 Enhanced redifferentiation of chondrocytes on microperiodic silk/gelatin scaffolds: toward tailor-made tissue engineering *Biomacromolecules* **14** 311–21
[31] Zhong N, Dong T, Chen Z, Guo Y, Shao Z and Zhao X 2019 A novel 3D-printed silk fibroin-based scaffold facilitates tracheal epithelium proliferation in vitro *J. Biomater. Appl.* **34** 3–11
[32] Zheng Z, Wu J, Liu M, Wang H, Li C, Rodriguez M J, Li G, Wang X and Kaplan D L 2018 3D bioprinting of self-standing silk-based bioink *Adv. Healthcare Mater.* **7** 1701026
[33] Jose R R, Brown J E, Polido K E, Omenetto F G and Kaplan D L 2015 Polyol-silk bioink formulations as two-part room-temperature curable materials for 3D printing *ACS Biomater. Sci. Eng.* **1** 780–8
[34] Costa J B, Silva-Correia J, Oliveira J M and Reis R L 2017 Fast setting silk fibroin bioink for bioprinting of patient-specific memory-shape implants *Adv. Healthcare Mater.* **6** 1701021
[35] Natoli M, Leoni B D, D'Agnano I, Zucco F and Felsani A 2012 Good Caco-2 cell culture practices *Toxicol. In Vitro* **26** 1243–6
[36] Fang J and Li H 2012 A facile way to tune mechanical properties of artificial elastomeric proteins-based hydrogels *Langmuir* **28** 8260–5
[37] Mahmoud S F and Bialkowski S E 1995 Laser-excited fluorescence of dityrosine *Appl. Spectrosc.* **49** 1669–76
[38] Hu X, Kaplan D and Cebe P 2006 Determining beta-sheet crystallinity in fibrous proteins by thermal analysis and infrared spectroscopy *Macromolecules* **39** 6161–70
[39] Nicell J A and Wright H 1997 A model of peroxidase activity with inhibition by hydrogen peroxide *Enzyme Microb. Technol.* **21** 302–10
[40] Hernández-Ruiz J, Arnao M B, Hiner A N P, García-Cánovas F and Acosta M 2001 Catalase-like activity of horseradish peroxidase: relationship to enzyme inactivation by H2O2 *Biochem. J.* **354** 107–14
[41] Rezende R A, Bartolo P J, Mendes A and Filho R M 2009 Rheological behavior of alginate solutions for biomanufacturing *J. Appl. Polym. Sci.* **113** 3866–71
[42] Shen A, Caldwell D, Ma A W K and Dardona S 2018 Direct write fabrication of high-density parallel silver interconnects *Addit. Manuf.* **22** 343–50
[43] Rössle M, Panine P, Urban V S and Riekel C 2004 Structural evolution of regenerated silk fibroin under shear: combined wide- and small-angle x-ray scattering experiments using synchrotron radiation *Biopolymers* **74** 316–27
[44] Patanwala H S, Hong D, Vora S R, Bognet B and Ma A W K 2018 The microstructure and mechanical properties of 3D printed carbon nanotube-polylactic acid composites *Polym. Compos.* **39** E1060–71